ASIA-PACIFIC SOLAR RESEARCH CONFERENCE

PEER REVIEWED
ASIA-PACIFIC
SOLAR RESEARCH CONFERENCE

A Preliminary Analysis for Development of a High-Temperature Gas-Phase Solar Receiver

Mohammadreza Sedighi and Ricardo Vasquez Padilla

School of Science, Environment and Engineering, Southern Cross University, Lismore Campus, NSW, Australia

E-mail: m.sedighi.10@student.scu.edu.au

Abstract

A preliminary study is used to develop a novel high-temperature pressurised non-windowed cavity receiver which utilises a compound Heat Transfer Enhancement (HTE) method. The cavity absorber is covered by impinging jets and extended surface techniques together to increase the solid absorber-to-HTF heat transfer rate and to keep the temperature of the cavity below the maximum service temperature of the cavity. Results showed that a compound technique of impinging jets on a plate-fin heat sink (compared to the impinging jets on a clean cavity and forced flow through a plate-fin heat sink) provides the highest convective heat transfer coefficient by around two times higher than the convection coefficient required to keep the temperature less than the cavity maximum working temperature.

1. Introduction

A state-of-art solar receiver feeds a Rankine power cycle with an outlet temperature up to 600˚C. However, to increase the efficiency, recent global interest has been fuelled for a sCO_2 Brayton cycle. This power cycle is able to provide efficiency even higher than 50%, if the inlet temperature is higher than 700˚C (Turchi, Ma et al. 2013). The main difference between a Rankine cycle and a Brayton cycle is that the working fluid in the former transforms within liquid to vapour among boiler (in a solarised cycle a heat exchanger is used instead), turbine and condenser, while the latter includes a compressor, combustion chamber and turbine with always gaseous working fluid (Nag 2013). In a solarised Brayton cycle, the combustion chamber can be eliminated (Turchi, Ma et al. 2013). Consequently, the new trend in CSP research aims to develop a solar receiver providing HTF outlet temperature above 700˚C to be efficiently integrated with a sCO2 Brayton cycle (Mehos, Turchi et al. 2016, Ho 2017, Mehos, Turchi et al. 2017). The current commercialised technologies include the first (direct steam) and second (thermal storage) generations of receiver, while the third generation, the integration of solar receiver with supercritical carbonate dioxide (sCO_2) Brayton cycle to generate low-cost electricity, is under development (Mehos, Turchi et al. 2017). A volumetric pressurised gas-phase solar receiver, due to a wide temperature range of its gaseous HTF, has this potential to provide such high temperature. This receiver uses a pressurised gaseous HTF, e.g. air or CO_2, flowing through a porous medium which is exposed to a direct irradiation flux. Through this process HTF is heated. In this directly-irradiated HTF cavity receiver type, a window is required to make the cavity receiver close-loop while it let the solar radiative flux come inside. However, the window needs to be strength enough for a long-term operation and also permanently needs to be clean and clear. To address these issues associated with use of a windowed cavity, concept of an indirectly-irradiated HTF receiver has recently grabbed the attention (Hischier, Leumann et al. 2012, Hischier, Poživil et al. 2012, Kim, Lee et al. 2014, Poživil, Aga et al. 2014, Pozivil, Ackermann et al. 2015, Poživil, Ettlin et al. 2015, Wang, Laumert et al. 2015, Wang, Wang et al. 2016, Giovannelli and Bashir 2017). In this type of receiver, the window is eliminated and cavity plays role as an absorber. The irradiative flux touches the aperture-facing surface of the cavity while the heat transfers to the HTF from the non-irradiated side. However, the heat transfer in this indirect irradiation HTF receiver is limited by cavity wall conductivity. Moreover, this type of receiver also suffers from a low heat transfer rate

between gaseous HTF and solid absorber due to intrinsically poor properties of a gaseous HTF which results in a low thermal efficiency and high temperature gradient throughout the cavity. This paper aims to preliminarily design and develop an indirectly-irradiated HTF cavity receiver using a Heat Transfer Enhancement technique to increase the absorber-HTF heat transfer rate and keep the temperature of the cavity below the maximum service temperature.

2. Material and Methods

A preliminary inverse design method (Wang, Xu et al. 2014) is used in this study to calculate the heat transfer coefficient required to remove the extra heat and keep the temperature below the maximum service temperature of the cavity material. This analysis includes two parts of calculation of required convection coefficient provided by mathematical heat transfer model and computation of convective flux through available Nusselt correlations. A 1-D mathematical model (Wang, Xu et al. 2014, Wang, Laumert et al. 2015, Wang, Wang et al. 2016) (Figure 1) is used to calculate the convective heat transfer coefficient required to remove the extra heat. In this inverse method, a uniform temperature distribution of inner surface of the cavity, which is based on the maximum service temperature of the cavity material, and an input solar radiative flux on the cylindrical cavity are considered as inputs to the heat transfer model. Finally, different Heat Transfer Enhancement (HTE) techniques are used to absorb the heat from non-heated side of the cavity in this study. In this part the average convection coefficient provided by these techniques are compared with the required convection coefficient calculated before. The two above-mentioned parts are briefly illustrated in Figure 2. The model is a 300mm-long cylindrical cavity with a diameter of 220mm and a thickness of 5mm. A silicon carbide has been widely used as an absorber in high-temperature receivers, either porous absorber or cavity absorber, due to its high maximum service temperature (Petrasch, Meier et al. 2008, Hischier, Leumann et al. 2012, Hischier, Poživil et al. 2012, Cheng, He et al. 2013, Daguenet-Frick, Toutant et al. 2013, Poživil, Aga et al. 2014, Wang, Xu et al. 2014, Aichmayer, Spelling et al. 2015, Chen, Xia et al. 2015, Hischier, Poživil et al. 2015, Pozivil, Ackermann et al. 2015, Poživil, Ettlin et al. 2015, Wang, Ragnolo et al. 2015, Ndiogou, Thiam et al. 2016, Giovannelli and Bashir 2017, Wang, Li et al. 2017). Accordingly, here a silicon carbide cavity absorber is used with a thermal conductivity of 26 W/(m K), an emissivity of 0.9 and a maximum service temperature of 1200˚C.

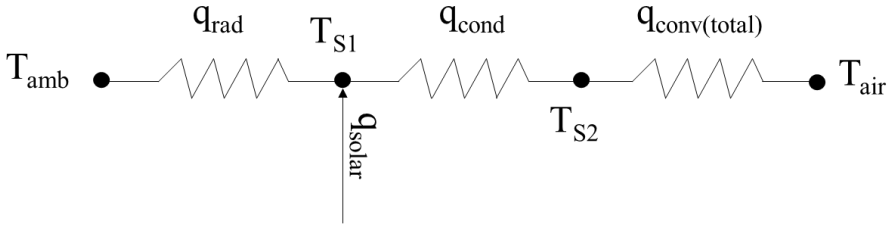

Figure 1. A 1-D thermal resistance circuit heat transfer model.

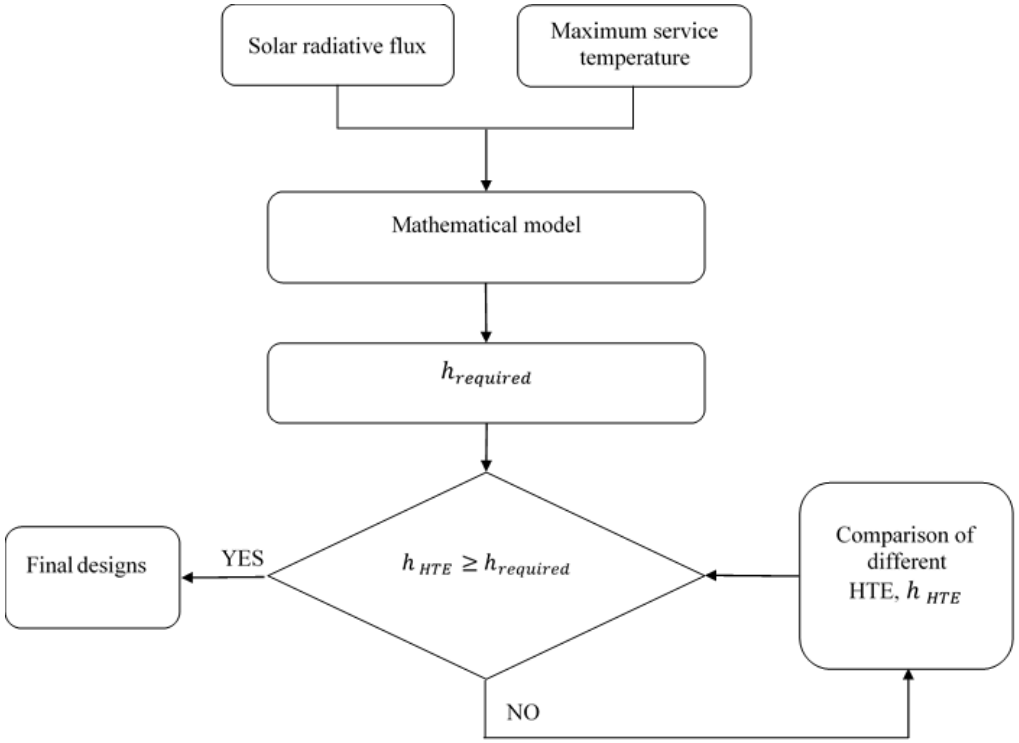

Figure 2. Flowchart of the method used in this paper.

Since there is an assumption of uniform temperature distribution over the cavity, radiative flux between different surfaces of the cavity is ignored. Hence, this model includes only cavity-to-ambient radiative heat transfer. The radiation heat transfer between the cavity and ambient is calculated by Eq. (1) and Eq. (2) (Wang, Xu et al. 2014, Wang, Wang et al. 2016).

$$Rad_{S1-amb} = \frac{\pi D_{S1}\sigma(T^4{}_{S1} - T^4{}_{amb})}{(1-\varepsilon_{S1})/\varepsilon_{S1} + 1/F_{S1-amb}} \quad (1)$$

$$F_{S1-amb} = \frac{\left(x/D_{S1}\right)^2 + 0.5}{\sqrt{\left(x/D_{S1}\right)^2 + 1}} - \left(x/D_{S1}\right) \quad (2)$$

where σ and F_{S1-amb} are Stephan-Boltzman constant and perimeter wall-to-ambient view factor and ε_{S1} and D_{S1} are emissivity and diameter of inner surface of the cavity, respectively.

One-dimensional cylindrical steady state conductive heat transfer is calculated by the following equation (Bergman, Incropera et al. 2011):

$$Cond_{S1-S2} = 2\pi k_s(T_{S1} - T_{S2})/\ln(\frac{D_{S2}}{D_{S1}}) \quad (3)$$

where T_{S1} and T_{S2} are temperature of inner and outer surfaces of the cavity, respectively. Also K_s is the thermal conductivity of the cavity material.

Since the gaseous HTFs suffer from a low conductivity (Benoit, Spreafico et al. 2016, Ho 2017), some improvements in fluid-absorber interaction are required. Several techniques have been utilised for heat transfer enhuncements which are categorised into two groups of passive and active methods. There are numerous comprehensive reviews available in the literature about HTE techniques including both passive and active methods (Siddique, Khaled et al. 2010, Liu and Sakr 2013, Sheikholeslami, Gorji-Bandpy et al. 2015, Xu, Sasmito et al. 2016, Sandeep and Arunachala 2017, Alam and Kim 2018). Here convective flow through a plate-fin heat sink, impinging jet on a clean surface and impinging jet on a plate-fin heat sink are compared. There are several correlations available in the literature for air impinging jet on a flat plate. However, there is a limited number of correlations available for jet impingement on a cylindrical target. Accordingly, it might be possible to use available correlations of flat plate rather than that of cylindrical target. Here a comparison will be done between convective heat transfers on a flat plate with a cylindrical target to find their differences.

Hofmann et al. (Hofmann, Kind et al. 2007) developed Nusselt correlation of jet impingement on a flat target for 14,000<Re<230,000 (Eq. (4)). Nusselt correlation for convective flow through a plate-fin heat sink (Eq. (5)) was proposed by Elshafei (Elshafei 2007) for 3000 < Re < 38000. For a plate-fin heat sink under an impinging jet, the following correlation was proposed (Eq. (6)) (Fubing, Jianfeng et al. 2011) for 3000<Re<16000. Figure 3 illustrates the schematic of these receivers analysed in this study.

$$Nu_{jet-clean\ surface} = 0.055(Re^3 + 10Re^2)^{0.25} Pr^{0.42}\, \mathrm{e}^{\left(-0.025*\left(\frac{r}{d}\right)^2\right)} \tag{4}$$

$$Nu_{plate-fin} = 7.552 \frac{Re^{0.182}}{\left((1+A)*(1+B)\right)^{0.1096}} \qquad A = \frac{C}{Hf} \quad B = \frac{C}{S} \tag{5}$$

$$Nu_{jet-plate-fin} = 0.56 Hf^{0.35} Re^{0.44} \left(\frac{H}{d}\right)^{0.25} Pr^{0.42} \tag{6}$$

where d is nozzle diameter, Hf is fin height and H is nozzle to cavity distance.

For impinging jet on a cylinder in a radial direction the following equation was proposed by Lee et al. (Lee, Chung et al. 1997) which has been widely used by several researchers:

$$Nu_{\text{cylinder}} = 0.6 Re^{0.6} \left(\frac{H}{d}\right)^{-0.2} \left(\frac{d}{D}\right)^{0.38} \tag{7}$$

where H is nozzle-to-convex distance and D is diameter of the convex. This correlation is valid within 11000< Re <50000, 0.034<$\frac{d}{D}$<0.089 and 2<$\frac{H}{d}$<6.

Sharif and Ramirez (Sharif and Ramirez 2013) numerically studied the impinging jet on a roughened convex with different grain roughness height and the results were presented in graphical forms. Here, we generated the following correlation as a function of Reynolds number and ratio of roughness height to cylindrical target diameter with a maximum 10% deviation using data analysis offered by Microsoft Excel:

$$Nu_{cylinder} = 0.012704Re^{0.934895}\left(\frac{K_{roughness}}{D}\right)^{0.018089} \quad (8)$$

where $K_{roughness}$ is the height of grain roughness and D is diameter of convex target. The correlation is valid over 13<d<34mm, 0.034<$\frac{d}{D}$<0.089, 0<$K_{roughness}$<1500μm and 11000< Re <50000. For smooth plate $K_{roughness}$ should be considered as low as possible.

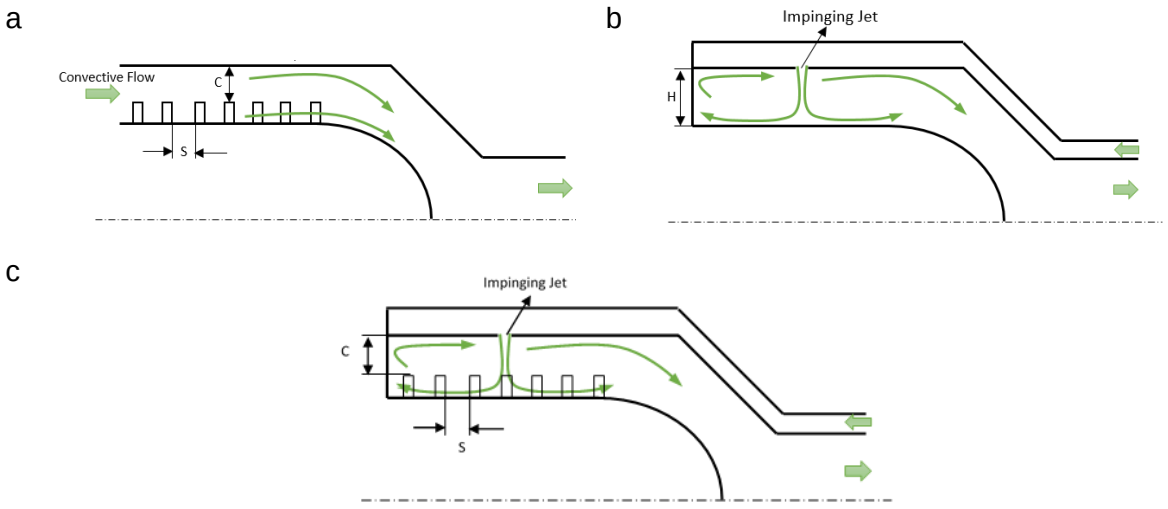

Figure 3. Schematic of the models: (a) cavity covered by a plate-fin under convective flow; (b) clean cavity exposed to impinging jets; (c) cavity with plate-fin exposed to impinging jets.

3. Results and discussions

3.1. Comparison of cylindrical target with flat target

There are limited numbers of Nusselt correlations for impinging jet on cylindrical targets. Lee et al. (Lee, Chung et al. 1999) demonstrated that the Nusselt number of impinging jet on a cylindrical target is higher than flat surface. Here, a comparison between Nusselt numbers for jet impingement on flat surface is done with that of convex target by using Eqs. (4), (7)-(8).

The correlations for convex surface are dependent on the ratio of nozzle diameter to cylinder diameter ($\frac{d}{D}$). When the ratio increases, Nusselt number of convex model decreases. Furthermore, the impinging flow spreads over the cylinder alongside the two axial and radial directions differently (Cornaro, Fleischer et al. 1999). Meanwhile, the correlations selected for this study need to be valid within the $\frac{d}{D}$ and Reynolds number used in our model. However, there is a lack of available correlations in the literature for impinging jet on a cylinder in both directions within our design points. Equations (7) and (8) which are valid within 0.034<$\frac{d}{D}$<0.089 and 11000<Re<50000 and including only radial flow direction are used here for the comparison.

Figure 4 demonstrates that jet impingement on a convex target (radial direction) provides around 9 to 17% higher Nusselt number compared with that of flat surface. The results are almost similar to the results of Lee et al. (Lee, Chung et al. 1999) who compared the stagnation and local Nusselt numbers of a flat with a convex hemispherical surfaces exposed to an impinging jet. Their results showed that the latter increases the Nusselt number by 6% to 12% compared with the flat target.

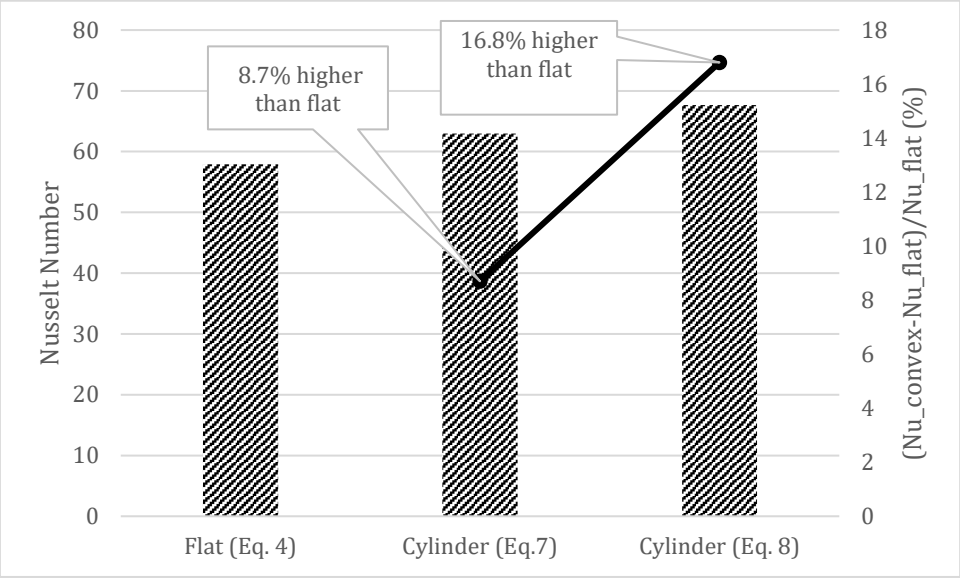

Figure 4. Nusselt numbers comparison of flat surface with convex surface for Re=23000, d=15mm, H/d=4 and d/D=0.056.

Figure 5 shows the variation of $\frac{d}{D}$ compared with the flat surface Nusselt number. The results shows when the ratio increases, Nusselt number of convex model decreases. When the ratio of nozzle diameter to cylinder diameter (d/D) is 0.045, the Nusselt number of a convex surface is almost same as that of a flat surface. In our model the diameter of cylinder is 220 mm. Therefore, the nozzle with a 10 mm diameter is chosen for this study.

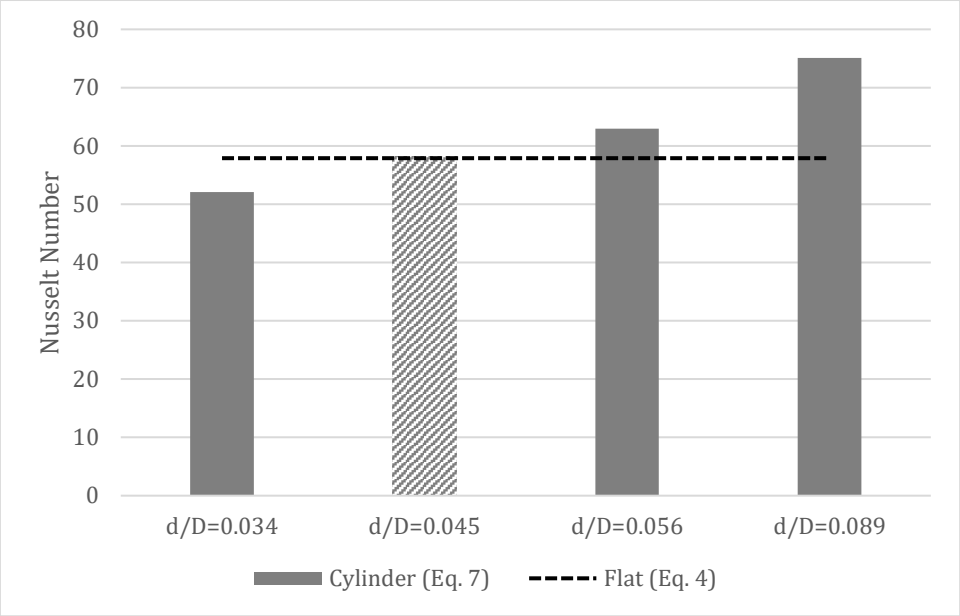

Figure 5. Nusselt numbers comparison of convex surface at different d/D with that of flat surface.

Moreover, since impinging jet on cylinder spreads on two sides of radial and axial directions differently, it is even expected that impinging jet on cylindrical target provides higher Nusselt number (Tawfek 1999). Hence, the correlations correspond to the flat target, which provides almost the same Nusselt number as that of cylinder or lower, will be applied for calculation of heat transfer coefficient in this paper as a conservative assumption.

3.2. Performance comparison of different HTE techniques on cavity

The convective heat transfer coefficient required to remove the extra heat in order to keep the temperature of the cavity below the working temperature limit of the cavity material is calculated according to the thermal resistance circuit (Figure 1) by using the equations (1) - (3) and programming in MatLab. Here, a uniform temperature distribution of 1200˚C is considered for the inner surface of the cavity selected according to its maximum service temperature and a 0.2 MW/m^2 input radiative flux. The required average amount of the convection coefficient calculated through the mathematical modelling is 357.17 W/(m^2 K). To absorb the heat from the non-heated surface of the cavity, HTF impinging jets on the clean cavity, plate-fin heat sink under a HTF convective flow and under a HTF impinging jets are used and their convection coefficients provided are compared with the required amount in order to find out which models are able to provide at least the required amount (Figure 6). The height of each fin is 10 mm and the tip-to-shroud clearance is 2 mm. The comparison is done for multiple jet impingements. If the ratio of nozzle-to-nozzle distance to the nozzle diameter ($\frac{Pitch_{jet}}{d_{jet}}$) is equal and greater than 8 and nozzle-to-cavity distance over its diameter ($\frac{H_{jet}}{d_{jet}}$) is greater than 2 then the interactions between the nozzles are negligible (Zuckerman and Lior 2006). Taken all cavity and nozzle diameters and above-mentioned conditions ($\frac{Pitch_{jet}}{d_{jet}} \geq 8$ and $\frac{H_{jet}}{d_{jet}} > 2$) together, it is possible to use 9 nozzles around the cavity. The comparison is made according to the same mass flow rate. Accordingly, the Reynolds number among plate-fin heat sink

under forced convective flow and round nozzle impinging jets are different. In addition, the operation pressure is 3 bar.

Figure 6 shows that the compound technique of impinging jets on a plate-fin provides the highest convective heat transfer coefficient while the plate-fin heat sink exposed to a forced convection flow has the lowest amount. This figure clearly demonstrates that impinging jet can be a more efficient solution to increase the efficiency and outlet temperature in a non-windowed cavity gas-phase receiver compared with use of a heat sink under a forced flow on non-heated side of the cavity absorber. Moreover, the heat transfer coefficient provided by impinging jets either on a clean surface or on a heat sink-covered surface almost can meet the requirement (dashed line) whereas the heat transfer coefficient provided by a plate-fin heat sink under a forced convective flow is lower than the convective heat transfer required to keep the temperature less than the maximum service temperature. The cavity covered by a plate-fin under a forced flow provided almost a third of the required amount, while convection coefficient of the impinging jet on the clean cavity is almost equal to the required amount and the impinging jets on pinned cavity is around two times higher than the requirement.

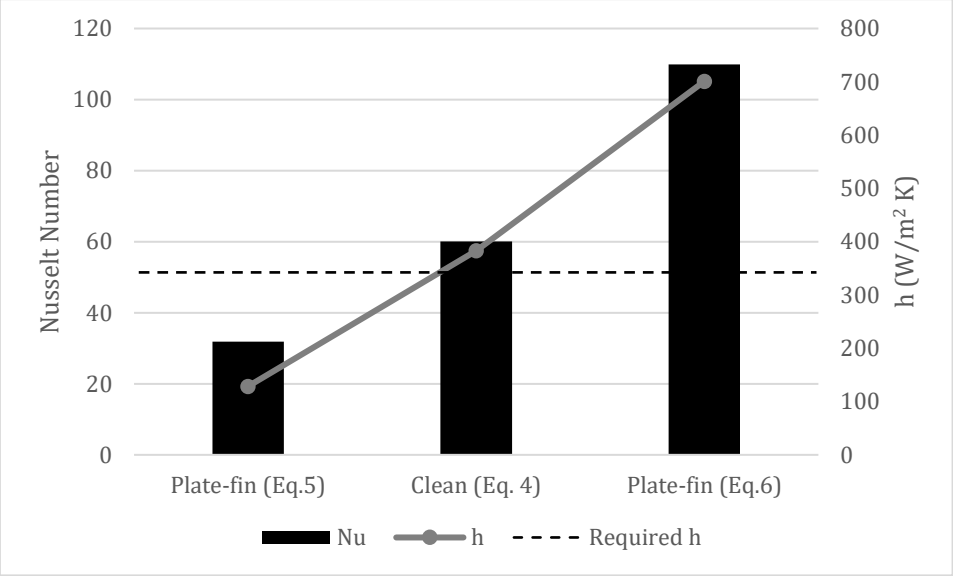

Figure 6. Average Nusselt numbers and convective heat transfer coefficients at mass flow rate of 0.0415 kg/s and nozzle diameter of 10 mm compared with the required convection coefficient (dashed line). .

An exclusive parametric study is done on the pinned plate under the impinging jets to optimise its performance through different fin heights and nozzle-to-cavity distances. Figure 7 shows that when the height of the fin increases from 0.3 to just above the 0.55 of the nozzle-to-cavity distance, Nusselt number and convection coefficient increases by around 25%. Similarly, increasing the ratio of nozzle-to-plate distance to nozzle diameter, in the same Reynolds number, results in an increase in both Nusselt number and convective heat transfer. However, when diameter of nozzle increases, while the H/d is constant, convective heat transfer decreases dramatically (Figure 8).

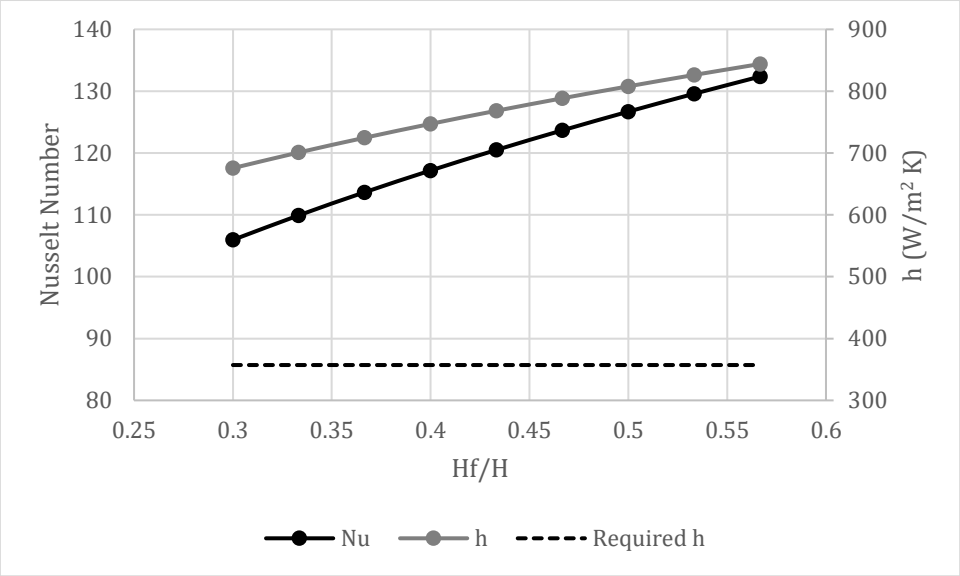

Figure 7. Average Nusselt numbers and convective heat transfer coefficients versus different fin height (solid line) compared with the required convection coefficient (dashed line).

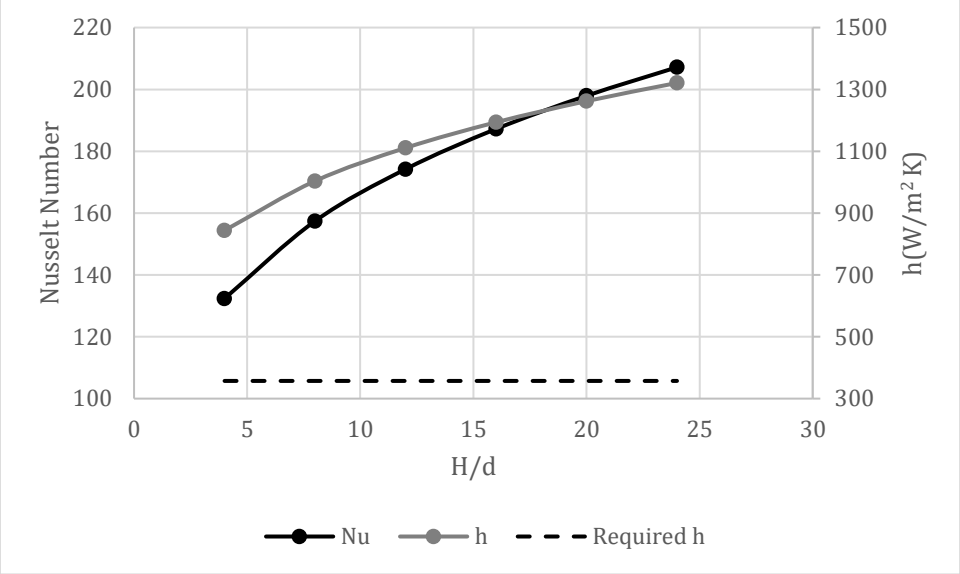

Figure 8. Average Nusselt numbers and convective heat transfer coefficients versus different nozzle-to-cavity distance (solid line) at Hf/H=0.56 compared with the required convection coefficient (dashed line).

4. Conclusion

In this study, an inverse heat transfer mathematical method was used to preliminarily design a pressurised, high-temperature, non-windowed cavity receiver. Convection coefficient required to keep the temperature of the cavity absorber below its maximum service temperature under a uniform solar radiative flux was calculated through mathematical modelling. Then, the available empirical correlations for calculation of Heat Transfer Enhancement (HTE) techniques convective flux, were

used to absorb the heat from non-heated side of the cavity. Active and passive HTE techniques were utilised in this study including nine impinging jets around the clean cavity and convective flow through a plate-fin heat sink. For further enhancements in HTF-absorber heat transfer rate, a compound HTE technique including impinging jets on a plate-fin heat sink was also proposed to be used. Results showed that when the compound technique was used, the highest amount of convective heat transfer coefficient was achieved by around 2 times higher than the required amount.

In the present study, the spatial variations of the radiative flux and temperature distributions are not included. For future research, a local solar radiative flux absorbed by the cylindrical cavity absorber computed by a ray-tracing analysis will be used as an input to the mathematical model to calculate the local temperature distribution and local convection coefficient required to keep the temperature less than its maximum service temperature. In addition, the effect of the different number of nozzles and diameters around the cavity on pressure drop and heat transfer will be studied to find the optimum arrangement.

References

Aichmayer, L., J. Spelling and B. Laumert (2015). "Preliminary design and analysis of a novel solar receiver for a micro gas-turbine based solar dish system." Solar Energy **114**: 378-396.
Alam, T. and M.-H. Kim (2018). "A comprehensive review on single phase heat transfer enhancement techniques in heat exchanger applications." Renewable and Sustainable Energy Reviews **81**: 813-839.
Benoit, H., L. Spreafico, D. Gauthier and G. Flamant (2016). "Review of heat transfer fluids in tube-receivers used in concentrating solar thermal systems: Properties and heat transfer coefficients." Renewable and Sustainable Energy Reviews **55**: 298-315.
Bergman, T. L., F. P. Incropera, D. P. DeWitt and A. S. Lavine (2011). Fundamentals of heat and mass transfer, John Wiley & Sons.
Chen, X., X.-L. Xia, X.-L. Meng and X.-H. Dong (2015). "Thermal performance analysis on a volumetric solar receiver with double-layer ceramic foam." Energy Conversion and Management **97**(Supplement C): 282-289.
Cheng, Z. D., Y. L. He and F. Q. Cui (2013). "Numerical investigations on coupled heat transfer and synthetical performance of a pressurized volumetric receiver with MCRT–FVM method." Applied Thermal Engineering **50**(1): 1044-1054.
Cornaro, C., A. S. Fleischer and R. J. Goldstein (1999). "Flow visualization of a round jet impinging on cylindrical surfaces." Experimental Thermal and Fluid Science **20**(2): 66-78.
Daguenet-Frick, X., A. Toutant, F. Bataille and G. Olalde (2013). "Numerical investigation of a ceramic high-temperature pressurized-air solar receiver." Solar Energy **90**(Supplement C): 164-178.
Elshafei, E. (2007). "Effect of flow bypass on the performance of a shrouded longitudinal fin array." Applied Thermal Engineering **27**(13): 2233-2242.
Fubing, T., M. Jianfeng, Z. Jiemin, Z. Wenhui, J. Yu and W. Huifen (2011). Heat Transfer from Rectangular Pin Fin Heat Sinks under Air Jet Impingement. Intelligent Computation Technology and Automation (ICICTA), 2011 International Conference on, IEEE.
Giovannelli, A. and M. A. Bashir (2017). "Development of a solar cavity receiver with a short-term storage system." Energy Procedia **136**: 258-263.
Giovannelli, A. and M. A. Bashir (2017). "High-Temperature Cavity Receiver Integrated with a Short-Term Storage System for Solar MGTs: Heat Transfer Enhancement." Energy Procedia **126**: 557-564.
Hischier, I., P. Leumann and A. Steinfeld (2012). "Experimental and numerical analyses of a pressurized air receiver for solar-driven gas turbines." Journal of Solar Energy Engineering **134**(2): 021003.

Hischier, I., P. Poživil and A. Steinfeld (2012). "A modular ceramic cavity-receiver for high-temperature high-concentration solar applications." Journal of solar energy engineering **134**(1): 011004.
Hischier, I., P. Poživil and A. Steinfeld (2015). "Optical and Thermal Analysis of a Pressurized-Air Receiver Cluster for a 50 MWe Solar Power Tower." Journal of Solar Energy Engineering **137**(6): 061002.
Ho, C. K. (2017). "Advances in central receivers for concentrating solar applications." Solar Energy **152**(Supplement C): 38-56.
Hofmann, H. M., M. Kind and H. Martin (2007). "Measurements on steady state heat transfer and flow structure and new correlations for heat and mass transfer in submerged impinging jets." International Journal of Heat and Mass Transfer **50**(19): 3957-3965.
Kim, H. N., H. J. Lee, S. N. Lee, J. K. Kim, K. K. Chai, H. K. Yoon, Y. H. Kang and H. S. Cho (2014). "Experimental evaluation of the performance of solar receivers for compressed air." Journal of Mechanical Science and Technology **28**(11): 4789-4795.
Lee, D., Y. Chung and D. Kim (1997). "Turbulent flow and heat transfer measurements on a curved surface with a fully developed round impinging jet." International Journal of Heat and Fluid Flow **18**(1): 160-169.
Lee, D. H., Y. S. Chung and M. G. Kim (1999). "Technical NoteTurbulent heat transfer from a convex hemispherical surface to a round impinging jet." International Journal of Heat and Mass Transfer **42**(6): 1147-1156.
Liu, S. and M. Sakr (2013). "A comprehensive review on passive heat transfer enhancements in pipe exchangers." Renewable and Sustainable Energy Reviews **19**: 64-81.
Mehos, M., C. Turchi, J. Jorgenson, P. Denholm, C. Ho and K. Armijo (2016). On the Path to SunShot. Advancing Concentrating Solar Power Technology, Performance, and Dispatchability, National Renewable Energy Lab.(NREL), Golden, CO (United States).
Mehos, M., C. Turchi, J. Vidal, M. Wagner, Z. Ma, C. Ho, W. Kolb, C. Andraka and A. Kruizenga (2017). Concentrating Solar Power Gen3 Demonstration Roadmap, NREL (National Renewable Energy Laboratory (NREL), Golden, CO (United States)).
Nag, P. (2013). Engineering thermodynamics, Tata McGraw-Hill Education.
Ndiogou, B. A., A. Thiam, C. Mbow, P. Stouffs and D. Azilinon (2016). Study and modeling of a pressurized air receiver to power a micro gas turbine. AIP Conference Proceedings, AIP Publishing.
Petrasch, J., F. Meier, H. Friess and A. Steinfeld (2008). "Tomography based determination of permeability, Dupuit–Forchheimer coefficient, and interfacial heat transfer coefficient in reticulate porous ceramics." International Journal of Heat and Fluid Flow **29**(1): 315-326.
Pozivil, P., S. Ackermann and A. Steinfeld (2015). "Numerical Heat Transfer Analysis of a 50 kWth Pressurized-Air Solar Receiver." Journal of Solar Energy Engineering **137**(6): 064504-064504-064504.
Poživil, P., V. Aga, A. Zagorskiy and A. Steinfeld (2014). "A Pressurized Air Receiver for Solar-driven Gas Turbines." Energy Procedia **49**(Supplement C): 498-503.
Poživil, P., N. Ettlin, F. Stucker and A. Steinfeld (2015). "Modular Design and Experimental Testing of a 50 kWth Pressurized-Air Solar Receiver for Gas Turbines." Journal of Solar Energy Engineering **137**(3): 031002-031002-031007.
Sandeep, H. M. and U. C. Arunachala (2017). "Solar parabolic trough collectors: A review on heat transfer augmentation techniques." Renewable and Sustainable Energy Reviews **69**: 1218-1231.
Sharif, M. A. R. and N. M. Ramirez (2013). "Surface roughness effects on the heat transfer due to turbulent round jet impingement on convex hemispherical surfaces." Applied Thermal Engineering **51**(1): 1026-1037.
Sheikholeslami, M., M. Gorji-Bandpy and D. D. Ganji (2015). "Review of heat transfer enhancement methods: Focus on passive methods using swirl flow devices." Renewable and Sustainable Energy Reviews **49**: 444-469.

Siddique, M., A.-R. Khaled, N. Abdulhafiz and A. Boukhary (2010). "Recent advances in heat transfer enhancements: a review report." International Journal of Chemical Engineering **2010**.
Tawfek, A. (1999). "Heat transfer due to a round jet impinging normal to a circular cylinder." Heat and mass transfer **35**(4): 327-333.
Turchi, C. S., Z. Ma, T. W. Neises and M. J. Wagner (2013). "Thermodynamic study of advanced supercritical carbon dioxide power cycles for concentrating solar power systems." Journal of Solar Energy Engineering **135**(4): 041007.
Wang, P., J. B. Li, F. W. Bai, D. Y. Liu, C. Xu, L. Zhao and Z. F. Wang (2017). "Experimental and theoretical evaluation on the thermal performance of a windowed volumetric solar receiver." Energy **119**(Supplement C): 652-661.
Wang, W., B. Laumert, H. Xu and T. Strand (2015). "Conjugate heat transfer analysis of an impinging receiver design for a dish-Brayton system." Solar Energy **119**: 298-309.
Wang, W., G. Ragnolo, L. Aichmayer, T. Strand and B. Laumert (2015). "Integrated Design of a Hybrid Gas Turbine-receiver Unit for a Solar Dish System." Energy Procedia **69**: 583-592.
Wang, W., B. Wang, L. Li, B. Laumert and T. Strand (2016). "The effect of the cooling nozzle arrangement to the thermal performance of a solar impinging receiver." Solar Energy **131**: 222-234.
Wang, W., H. Xu, B. Laumert and T. Strand (2014). "An inverse design method for a cavity receiver used in solar dish Brayton system." Solar Energy **110**: 745-755.
Xu, P., A. P. Sasmito, S. Qiu, A. S. Mujumdar, L. Xu and L. Geng (2016). "Heat transfer and entropy generation in air jet impingement on a model rough surface." International Communications in Heat and Mass Transfer **72**: 48-56.
Zuckerman, N. and N. Lior (2006). "Jet impingement heat transfer: physics, correlations, and numerical modeling." Advances in heat transfer **39**: 565-631.